

Analysis of Combustion Noise in an Open Turbulent Spray Flame Using DNS: Effect of Radiative Heat Loss

Abhishek L. Pillai

Department of Mechanical Engineering and Science
Kyoto University
Kyoto daigaku-Katsura, Nishikyo-ku,
Kyoto 615-8540, Japan
pillai.abhishek.43c@st.kyoto-u.ac.jp

Ryoichi Kurose

Department of Mechanical Engineering and Science
Kyoto University
Kyoto daigaku-Katsura, Nishikyo-ku,
Kyoto 615-8540, Japan
kurose@mech.kyoto-u.ac.jp

ABSTRACT

Combustion noise generation from an open turbulent spray flame with Ethanol as the fuel is investigated using Direct Numerical Simulation (DNS). The multiphase reactive flow is simulated using an Eulerian/Lagrangian approach. The governing equations for the carrier gas phase are solved in an Eulerian framework, whereas the motions of the evaporating Ethanol droplets are tracked in a Lagrangian framework. A two-step global reaction mechanism is used to model Ethanol combustion. Two simulations are performed, one without considering radiative heat loss from the flame, while the other in which radiative heat loss is accounted for using an optically thin radiation model. The influence of radiative heat loss on the statistical flow field quantities and combustion noise is also investigated. The DNS results for velocity statistics of droplets show an overall good agreement with measurements and are virtually unaffected by the radiative heat loss source term, however the predictions for gas-phase excess temperature improve by taking radiative heat loss into consideration and show acceptable agreement with experimental data. The spectral content of the noise generated by the spray flame is broadband in nature. Furthermore, analysis of the noise directivity of the open turbulent spray flame indicates dominance of the monopole combustion noise sources due to the fluctuating heat release rate. Spectral content of combustion noise obtained from both simulations (with and without radiative heat loss) show subtle differences, but the range of noise intensities remain virtually similar for both cases indicating only a minor influence of the radiative heat loss on combustion generated noise. Furthermore, gradual suppression of noise emissions at high frequencies is observed with decreasing emission angle with respect to the flame axis in both cases.

INTRODUCTION

Commercial gas turbine engines are widely used for industrial power generation and aircraft propulsion in the form of ground based gas turbines and aeroengines, respectively. Heat addition inside the combustors of these engines occurs through the turbulent combustion of fuel that is often introduced inside the combustors in the form of liquid fuel sprays. However, this turbulent combustion of fuel generates a substantial amount of undesirable noise, referred to as combustion noise. For combustion occurring in confinement, as is the case for combustors, the total noise generated consists of direct and indirect combustion noise (Strahle, 1978). Direct combustion noise is produced by sources originating from the interaction between turbulence and chemical reactions that create heat release rate fluctuations (Strahle, 1978). The heat release rate fluctuations cause unsteady volumetric expansion and contraction of the reacting gases. On the other hand, indirect combustion noise arises when the entropy inhomogeneities (hot and cold spots) and vorticity inhomogeneities get accelerated as they are transported through the nozzle at the combustor outlet (Howe, 2010). Recently, emphasis

on the development of efficient lean-burn combustors with reduced emissions of NO_x and greenhouse gases has increased. However, the noise emission from lean combustion is substantially louder, because it is inherently more unsteady (Dowling & Stow, 2003). Hence, combustion noise is one of the dominant sources of engine core noise (Strahle, 1978). Apart from manifesting itself as noise pollution in the environment, combustion noise is also responsible for a far more serious problem in gas turbine engines, viz. thermo-acoustic instability or combustion instability (Candel, 2002). Investigations (both experimental and numerical) regarding the combustion noise generation in open turbulent spray flames are lacking in existing literature, let alone the noise generation in confined spray flames which is even more sophisticated. Hence, a better understanding of the combustion noise characteristics in turbulent spray flames/combustion is needed to clarify the underlying mechanism, and to improve combustor designs in order to reduce noise emissions and to prevent the induction of thermo-acoustic instabilities. In this study, DNS of an open turbulent spray flame designated "EtF3" with Ethanol as the fuel, are performed. This flame has been experimentally investigated by Gounder *et al.* (2012) at the University of Sydney. Since, the spray flame is unconfined, the direct combustion noise generated from it is analysed by studying the spectral content of the noise. Furthermore, the effect of radiative heat loss on the statistical flow field quantities and combustion noise is also examined by performing two simulation cases, one without considering radiative heat loss from the flame, and the second one in which radiative heat loss is taken into account using an optically thin radiation model (Grosshandler, 1993; Barlow *et al.*, 2001).

DIRECT NUMERICAL SIMULATION

For DNS of the turbulent spray flame, the carrier gas-phase is treated as an Eulerian continuum, while the dispersed fuel droplets are treated as point masses and tracked in a Lagrangian framework. Description of the Eulerian-Lagrangian framework employed in the simulations is now presented.

Governing Equations of Carrier Gas Phase

The gas-phase is solved in an Eulerian framework and its governing equations are the conservation equations for mass, momentum, energy, and species mass fraction expressed as

$$\frac{\partial \rho}{\partial t} + \nabla \cdot (\rho u) = S_\rho \quad (1)$$

$$\frac{\partial \rho u}{\partial t} + \nabla \cdot (\rho u u) = -\nabla P + \nabla \cdot \tau + S_{\rho u} \quad (2)$$

$$\frac{\partial \rho h}{\partial t} + \nabla \cdot (\rho h u) = \frac{DP}{Dt} + \nabla \cdot (\rho D_h \nabla h) + \tau : \nabla u + S_{rad} + S_{\rho h} \quad (3)$$

$$\frac{\partial \rho Y_k}{\partial t} + \nabla \cdot (\rho Y_k u) = \nabla \cdot (\rho D_k \nabla Y_k) + S_{comb,k} + S_{\rho Y_k} \quad (4)$$

along with the equation of state for ideal gas. In Eqs. (1) - (4), ρ is the density, u is the velocity vector, P is the pressure, τ is the stress tensor, h is the specific enthalpy, and Y_k is the mass fraction of k^{th} chemical species. The gaseous thermal diffusivity D_h is calculated by $D_h = \lambda / (\rho c_p)$, where λ is the thermal conductivity and c_p is the specific heat at constant pressure. The mass diffusion coefficient of k^{th} species D_k is given by $D_k = \lambda / (\rho c_p)$ assuming unity Lewis number ($Le = 1$). $S_{comb,k}$ is the reaction source term for k^{th} species and S_{rad} is the source term accounting for radiative heat loss.

Furthermore, phase coupling between the gas-phase and dispersed-phase (fuel droplets) is realized by employing the Particle-Source-In-Cell (PSI-Cell) approach (Crowe *et al.*, 1977), and the evaluation procedure of the source terms for fuel droplets S_{ρ} , $S_{\rho u}$, $S_{\rho h}$, and $S_{\rho Y_k}$ in Eqs. (1) - (4) are detailed in (Nakamura *et al.*, 2005; Kitano *et al.*, 2014, 2016).

Governing Equations of Fuel Droplets

The evaporating fuel droplets constituting the dispersed-phase are tracked individually in a Lagrangian framework by solving the droplet equations for position x_d , velocity u_d , temperature T_d , and mass m_d as follows

$$\frac{dx_d}{dt} = u_d \quad (5)$$

$$\frac{du_d}{dt} = \frac{f_1}{\tau_d} (u - u_d) \quad (6)$$

$$\frac{dT_d}{dt} = \left(\frac{Nu}{3Pr} \right) \left(\frac{c_p}{c_{p,d}} \right) \left(\frac{f_2}{\tau_d} \right) (T - T_d) + \frac{1}{m_d} \left(\frac{dm_d}{dt} \right) \frac{L_V}{c_{p,d}} \quad (7)$$

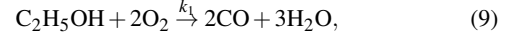
$$\frac{dm_d}{dt} = - \left(\frac{Sh}{3Sc} \right) \frac{m_d}{\tau_d} \ln(1 + B_M). \quad (8)$$

Here, T is the gas-phase temperature, c_p is the specific heat of gas, $c_{p,d}$ is the specific heat of fuel droplets, and L_V is the latent heat of vaporization at T_d . Pr is the Prandtl number defined by $Pr = \mu c_p / \lambda$, where μ is the gas-phase viscosity. Sc is the Schmidt number defined by $Sc = \mu / (\rho D_k)$. Nu , Sh , B_M and τ_d are the Nusselt number, Sherwood number, Mass transfer number and droplet response time, respectively, and are defined in (Bellan & Harstad, 1987; Miller *et al.*, 1998; Miller & Bellan, 1999; Nakamura *et al.*, 2005; Kitano *et al.*, 2014). The corrections of the Stokes drag and the heat transfer for an evaporating droplet are given by f_1 and f_2 , respectively. Descriptions of f_1 and f_2 are detailed in (Nakamura *et al.*, 2005; Miller *et al.*, 1998; Watanabe *et al.*, 2007). For the evaporation of fuel droplets, a non-equilibrium Langmuir-Knudsen evaporation model (Bellan & Harstad, 1987; Miller *et al.*, 1998; Miller & Bellan, 1999) is adopted.

Reaction Model

For the flame under consideration, Ethanol (C_2H_5OH) is used as liquid spray fuel. To describe the combustion of gaseous Ethanol using detailed reaction mechanism would prove to be computationally very expensive. Hence, a two-step global reaction mechanism (Westbrook & Dryer, 1981) is used to prescribe Ethanol combustion

as follows



Here, k_1 is the rate of Ethanol oxidation reaction in Eq. (13) and k_2 is the rate of forward reaction for CO oxidation in Eq. (14). The reaction rates expressed as modified Arrhenius formulations (Westbrook & Dryer, 1981) are

$$k_1 = 1.8 \times 10^{12} \exp\left(\frac{-30}{RT}\right) [C_2H_5OH]^{0.15} [O_2]^{1.6} \quad (11)$$

$$k_2 = 10^{14.6} \exp\left(\frac{-40}{RT}\right) [CO]^1 [H_2O]^{0.5} [O_2]^{0.25} \quad (12)$$

And, the reverse reaction in Eq. (14) has a rate k_{-2} (Westbrook & Dryer, 1981) that is defined as follows

$$k_{-2} = 5 \times 10^8 \exp\left(\frac{-40}{RT}\right) [CO_2]^1 \quad (13)$$

This two-step global reaction model provides a more accurate estimation of the flame parameters as compared to a one-step global reaction model (Westbrook & Dryer, 1981).

Radiation Model

The source term S_{rad} in the governing equation for energy conservation, i.e. Eq. (3) accounts for the radiative heat loss rate per unit volume. It is modelled using an optically thin approximation (Grosshandler, 1993; Barlow *et al.*, 2001) of radiative heat transfer between a fluid element in the flame and the cold surroundings. The radiative loss S_{rad} is estimated as

$$S_{rad} = 4\sigma (T^4 - T_b^4) \left[\sum_k p_k a_{p,k} \right] \quad (14)$$

Where $\sigma = 5.669e-08$ [W/m²K⁴] is the Stefan-Boltzmann constant, T is the gas phase/flame temperature, T_b is the background temperature and is assumed to be 300 K, p_k is the partial pressure of k^{th} chemical species in atmospheres, and $a_{p,k}$ is the Planck mean absorption coefficient for the k^{th} species. The Planck mean absorption coefficients have been evaluated using RADCAL (Grosshandler, 1993) and the curve fits of $a_{p,k}$ for the radiating species considered in this model namely, CO₂, H₂O and CO, are expressed as polynomial functions of temperature and documented in (Grosshandler, 1993; Barlow *et al.*, 2001).

COMPUTATIONAL DETAILS

The open turbulent Ethanol spray flame designated EtF3 has been experimentally investigated using a laboratory scale piloted spray burner by Gounder *et al.* (2012) at the University of Sydney. Fuel spray and carrier air issue out of a central jet nozzle which is surrounded by a coaxial pilot annulus and an outer stream of co-flowing air. The spray flame is stabilized by the pilot flame holder. The Ethanol spray flames parameters measured at the burner exit (for central jet nozzle and pilot flame) are listed in Table 1 and

Table 1. Flow parameters for central jet nozzle and pilot flame at burner exit.

Flame	EtF3
Fuel	Ethanol
Jet diameter, D [mm]	10.5
Pilot diameter [mm]	25
Bulk jet velocity, U_{jet} [m/s]	24
Bulk velocity pilot (burned) [m/s]	11.6
Bulk velocity co-flow stream [m/s]	4.5
Carrier air mass flow rate [g/min]	150
Liquid fuel injection rate [g/min]	45
Measured liquid flow at exit [g/min]	30.7
Vapour fuel flow rate at exit [g/min]	14.3
Jet Reynolds number, (Re)	19,700
Equivalence ratio at jet exit, ϕ_{exit} [-]	0.85
Pilot temperature [K]	2493

the same parameters are used for the DNS. The pilot consists of the fully-burned product of the stoichiometric mixture of 5.08% Acetylene (C_2H_2), 10.17% Hydrogen (H_2) and 84.75% air by volume and its adiabatic flame temperature is 2493 K. Further details regarding the burner setup and pilot flame holder are available in (Gounder *et al.*, 2012). DNS is performed for two cases, one without considering the radiative heat loss from the flame, and the other in which the radiative heat loss source term S_{rad} is accounted for. The DNS are performed on a staggered Cartesian grid consisting of $1160 \times 400 \times 400$ grid points (a total of 185.6 million points) in the x -, y - and z -directions, respectively. The minimum mesh spacing used is $150 \mu m$. The domain size is approximately $94D \times 49D \times 49D$ in the x -, y - and z -directions, respectively. The CPU time for each case is approximately 427500 hours by parallel computation using 1024 cores. Dispersed fuel droplets are randomly injected from the central jet nozzle with droplet sizes in the range of $1 \mu m - 70 \mu m$. Size distribution of the injected fuel droplets is prescribed using a Log-normal Probability Density Function (PDF) obtained from the best fit curve of experimental droplet size distribution data.

NUMERICAL PROCEDURE

The DNS are performed using an in-house thermal flow analysis code FK³ (Kitano *et al.*, 2014, 2016; Pillai *et al.*, 2016) whose algorithm consists of a fractional-step method, which employs a pressure-based semi-implicit algorithm for compressible flows (Moureau *et al.*, 2007). The spatial derivatives of the convective terms in the momentum equation are approximated using a 6th order accurate central difference scheme, while the convective terms in the governing equations of the scalar quantities are evaluated using the Weighted Essentially Non-Oscillatory (WENO) scheme (Jiang & Shu, 1996). The spatial derivatives of the stress tensor terms are evaluated using a 4th order central difference scheme and those of the diffusive terms are discretized by a 2nd order central difference scheme. The time integration of the convective terms is performed using a 3rd order explicit TVD Runge-Kutta method. Additionally, all the thermodynamic properties and transport coefficients tak-

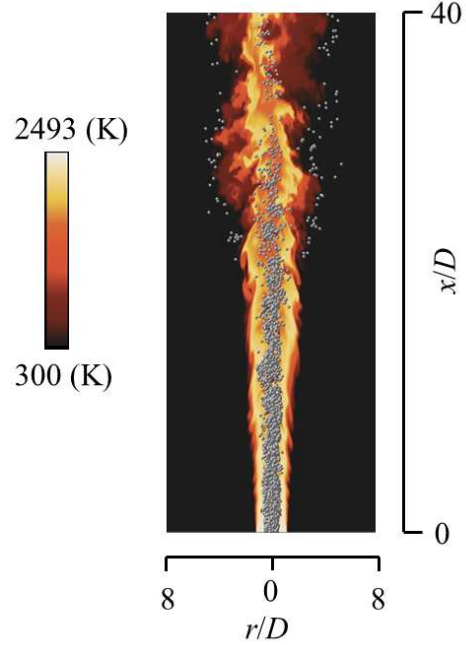


Figure 1. Instantaneous gas-phase temperature field computed with DNS along with the dispersed Ethanol droplets for the turbulent spray flame.

ing temperature dependence into consideration are obtained from CHEMKIN (Kee *et al.*, 1986, 1989). The radial profiles of gas-phase mean velocity, gas-phase turbulence intensity, and radial profiles of droplet mean velocities measured at the nozzle-exit plane are used as the inlet boundary conditions. Additionally, for the central spray nozzle transient turbulent fluctuations generated using a digital filter based technique (Klein *et al.*, 2003; Kempf *et al.*, 2012) are superimposed on the radial profile of gas-phase mean velocity at the nozzle exit to simulate pseudo turbulence. For the region outside pilot annulus exit (i.e. for $r/D > 25$ mm) at the inflow plane, the radial and azimuthal velocities are set to zero, the axial co-flow velocity of 4.5 m/s is imposed, and Neumann condition is applied to other physical quantities. At the outflow and lateral boundaries, the Neumann condition is imposed for all physical quantities. To minimize the amplitude of spurious waves reflected at the boundaries of the computational domain, a sponge zone combining grid stretching and Laplacian filtering (Bogey & Bailly, 2002) is used in the outflow direction (to dissipate the flow fluctuations before they reach the outflow boundary), while absorbing layers consisting of grid stretching and damping terms (artificial dissipation through filtering) are implemented for the lateral boundaries of the computational domain.

RESULTS AND DISCUSSION

Flow-Field

Fig. 1 shows the instantaneous gas-phase temperature field along with the dispersed fuel droplets obtained from DNS representing the predicted spray flame structure. The DNS results for the flow-field statistical quantities are validated against experimental measurements to assess the fidelity of the DNS. It was found that the inclusion of radiative heat loss source term S_{rad} in Eq. (3) did not show any appreciable change in the velocity statistics for the gas-phase and dispersed droplet phase from the simulation case without S_{rad} . Hence, the results for radial profiles of velocity statistics obtained from the simulation case taking S_{rad} into consideration alone, are presented in Figs. 2 and 3. Fig. 2 shows the radial profiles of

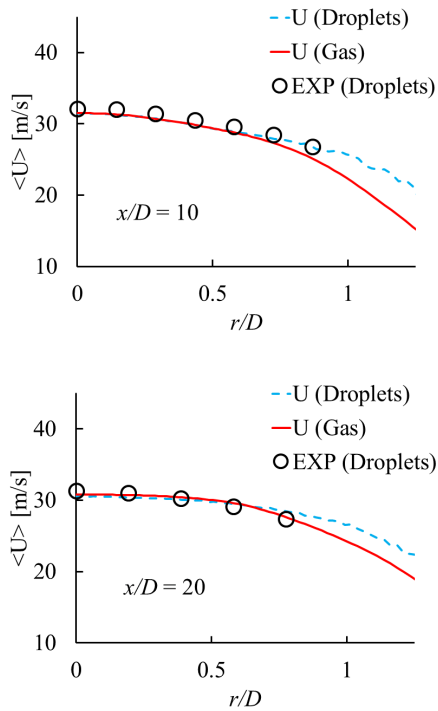


Figure 2. Radial profiles of droplet averaged axial velocity and mean gas-phase velocity compared with measurements at different stream-wise locations.

droplet averaged axial velocity as well as mean gas-phase velocity compared with measurements for different stream-wise positions. Similarly, Fig. 3 shows the radial profiles of RMS velocity fluctuations for droplets and gas-phase compared with measurements. The DNS results show good agreement with experimental findings with the flame spreading being well captured.

Additionally, radial profiles of gas-phase excess temperature at various stream-wise locations are presented in Fig. 4. Here, results obtained from both simulation cases (with and without S_{rad}) are shown and it is evident that the temperature predictions improve by taking the radiative heat loss into consideration. Some discrepancies in the predicted temperatures, especially at $x/D = 10$ are attributed to the limitations of the two-step global reaction model which can over-predict flame temperatures and delay ignition (under-predicted temperature near flame axis) (Westbrook & Dryer, 1981). Overall good agreement is observed with experiment and the temperature trends are well reproduced.

Combustion Noise

Experimental data for noise emission from the EtF3 spray flame are currently unavailable in literature, however the combustion noise generated by an open turbulent non-premixed Hydrogen flame (Brick *et al.*, 2005) has been validated in our previous work (Pillai *et al.*, 2016) using DNS employing the same in-house code FK³ and similar numerical procedure. Therefore, analyses of the combustion noise for EtF3 spray flame are performed. The computational grid used here is capable of resolving a maximum frequency of 5800 Hz assuming speed of sound in air with a conservative estimate of 22 points per wavelength. The DNS are executed with a constant time increment of $\Delta t = 6 \times 10^{-7}$ s, so the Nyquist frequency of temporal resolution is about 833.333 KHz that is much larger than the spatial resolution.

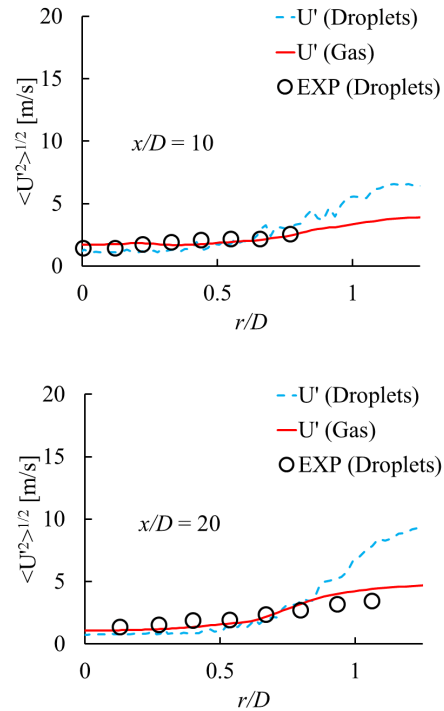


Figure 3. Radial profiles for RMS fluctuations of axial velocity of droplets and gas-phase compared with measurements at different stream-wise locations.

The effect of radiative heat loss source term S_{rad} on combustion noise is first investigated. Fig. 5 shows the computed sound intensity spectra for two locations outside the flame, $(x/D; r/D) = (17.32; 10)$ and $(5.8; 10)$ corresponding to emission angles of $\theta = 30^\circ$ and 60° , respectively to the flame axis, for both simulation cases (solid lines for DNS without S_{rad} and dashed lines for DNS with S_{rad}). The spectra are broadband and the spectral content show subtle differences between the two DNS cases. However, the range of sound intensity levels are practically unaltered which exhibits inconsequential effect of the radiative heat loss term S_{rad} on the combustion noise of this spray flame. This finding is further supported by the results in Fig. 6, which shows the stream-wise distributions of RMS fluctuations of heat release rate Q' for both DNS cases. The combustion noise sources arise from the heat release rate fluctuations (Strahle, 1978) and the magnitude of Q' remains virtually similar in both cases with minor influence of radiative heat loss S_{rad} .

Next, the noise directivity characteristics are investigated for both DNS cases. This is depicted in Fig. 7 which illustrates the sound intensity spectra computed at various locations outside the flame, viz. $(x/D; r/D) = (17.32; 10)$, $(12; 10)$, $(8.4; 10)$, $(5.8; 10)$ and $(3.64; 10)$ corresponding to emission angles of $\theta = 30^\circ$, 40° , 50° , 60° and 70° , respectively to the flame axis. The spectra are broadband in both DNS cases, the spectral content and sound intensities are fairly similar for all emission angles at the low and mid-frequencies (up to 2500 Hz). This shows the dominance of the distributed monopole-type combustion noise sources in EtF3 spray flame. However, for the higher frequencies (beyond 2500 Hz) suppression of sound intensities with decreasing emission angle θ is evident and this is represented by the green dashed-dotted lines in Fig. 7, which indicate the decrease in sound intensity levels for the high-frequency noise emissions from $\theta = 70^\circ$ to $\theta = 30^\circ$ in both cases. The downstream suppression of high frequency noise emissions is caused by refraction effects due to temperature gradients within the

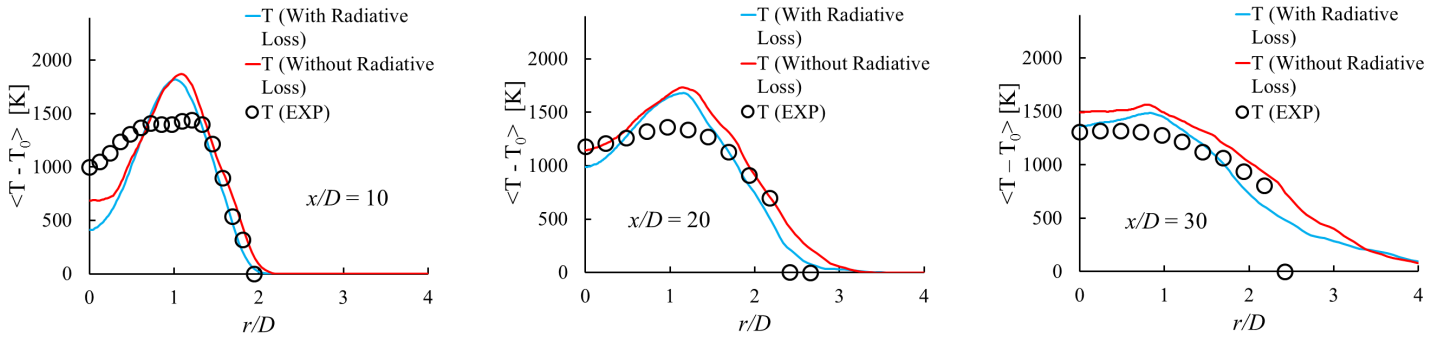
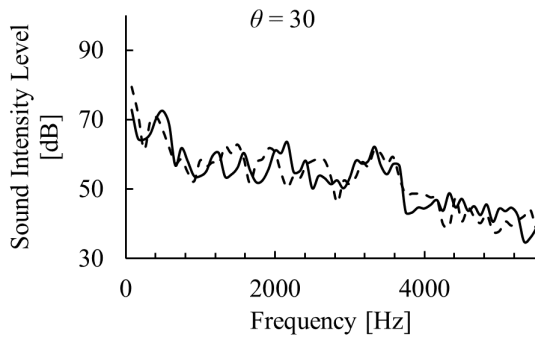
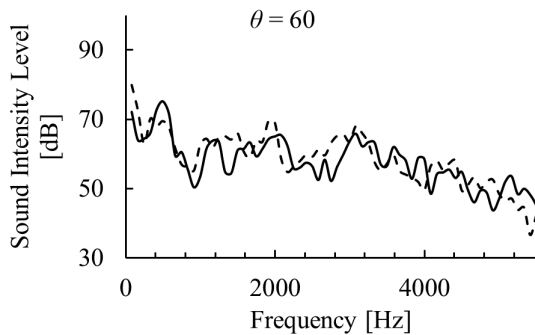


Figure 4. Radial profiles of gas-phase excess temperature at various stream-wise locations, T_0 is the ambient temperature ($T_0 = 293.15$ K).



(a)



(b)

Figure 5. Sound intensity level spectra computed at (a) $(x/D; r/D) = (17.32; 10)$ corresponding to emission angle $\theta = 30^\circ$ and (b) $(x/D; r/D) = (5.8; 10)$ corresponding to emission angle $\theta = 60^\circ$ to the flame axis, solid lines represent the spectra computed for the case without radiative heat loss and dashed lines for the case with radiative heat loss.

flame. Such acoustic refractions due to temperature-dependent variations in the speed of sound become increasingly significant with decreasing emission angle to the flame axis (Singh *et al.*, 2004; Ihme *et al.*, 2009). Therefore, the high frequency acoustic waves propagating in the downstream direction, upon interaction with the sound speed gradients get refracted away from the flame axis.

CONCLUSIONS

DNS was used to investigate the combustion noise generation from an open turbulent spray flame with Ethanol as the fuel. Two

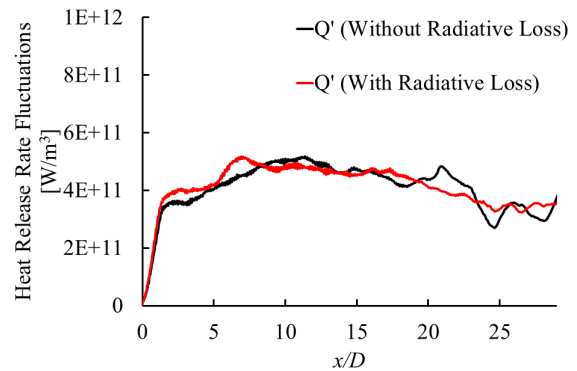
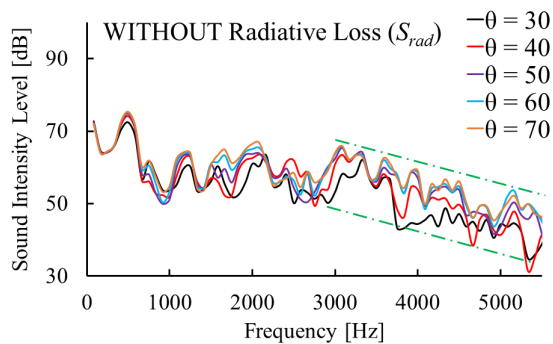


Figure 6. Stream-wise distributions of RMS fluctuations of heat release rate for both simulation cases (with and without radiative heat loss source term S_{rad}).

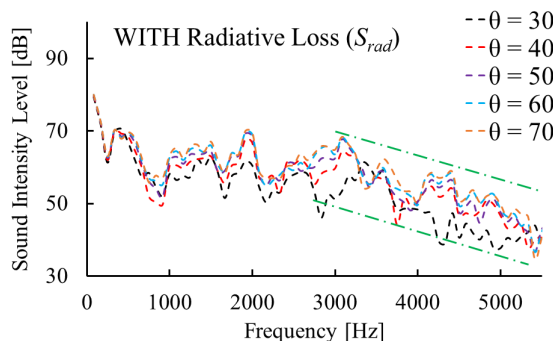
DNS were performed, one without considering radiative heat loss from the flame, and the other in which radiative heat loss was taken into account using an optically thin approximation. The DNS results for flow-field statistical quantities like droplet and gas-phase velocities, and gas-phase excess temperature showed an overall good agreement with measurement. By taking the radiative heat loss source term into consideration, the predictions for gas-phase excess temperature improved. The noise generated by the spray flame was found to be broadband. Subtle differences were observed in the spectral content of combustion noise obtained from both simulations, but the range of noise intensities remained practically similar for both cases. Hence, the influence of radiative heat loss on combustion generated noise was found to be inconsequential. Analysis of the noise directivity characteristics of the spray flame showed fairly similar spectral content and sound intensities at various emission angles to the flame axis for the low and mid-frequencies, which indicated the dominance of distributed monopole combustion noise sources arising from unsteady heat release rate fluctuations. However, suppression of the high frequency noise emissions with decreasing emission angle to the flame axis was observed which was attributed to the refraction effects due to temperature-dependent variations in the sound speed within the flame.

ACKNOWLEDGEMENTS

This research was supported by MEXT (Ministry of Education, Culture, Sports, Science, and Technology) as "Priority issue on Post-K computer" (Accelerated Development of Innovative Clean



(a)



(b)

Figure 7. DNS computed sound intensity level spectra for simulations (a) Without radiative heat loss source term and (b) With radiative heat loss source term, at various emission angles to the flame axis. The green dashed-dotted lines indicate the decrease in sound intensity levels for the high-frequency emissions with decreasing emission angle θ .

Energy Systems).

REFERENCES

- Barlow, R. S., Karpetis, A. N., Frank, J. H. & Chen, J.-Y. 2001 Scalar profiles and soot formation in laminar opposed-flow partially premixed methane/air flames. *Combustion and Flame* **127**, 2102–2118.
- Bellan, J. & Harstad, K. 1987 Analysis of the convective evaporation of nondilute clusters of drops. *International Journal of Heat and Mass Transfer* **30** (1), 125–136.
- Bogey, C. & Bailly, C. 2002 Three-dimensional non-reflective boundary conditions for acoustic simulations: Far field formulation and validation test cases. *Acta Acustica United with Acustica* **88**, 463–471.
- Brick, H., Piscocoya, R., Ochmann, M. & Költzsch, P. 2005 Prediction of the sound radiation from open flames by coupling a large eddy simulation and a Kirchhoff-method. *Acta Acustica united with Acustica* **91**, 17–21.
- Candel, S. 2002 Combustion dynamics and control: Progress and challenges. *Proceedings of the Combustion Institute* **29**, 1–28.
- Crowe, C. T., Sharma, M. P. & Stock, D. E. 1977 The Particle-Source-In Cell (PSI-CELL) model for gas-droplet flows. *Journal of Fluids Engineering* **99**, 325–332.
- Dowling, A. P. & Stow, S. R. 2003 Acoustic analysis of gas turbine combustors. *Journal of Propulsion and Power* **19**, 751–764.
- Gounder, J. D., Kourmatzis, A. & Masri, A. R. 2012 Turbulent piloted dilute spray flames: Flow fields and droplet dynamics. *Combustion and Flame* **159**, 3372–3397.
- Grosshandler, W. L. 1993 RADCAL: A narrow-band model for radiation calculations in a combustion environment. NIST Technical Note 1402.
- Howe, M. S. 2010 Indirect combustion noise. *Journal of Fluid Mechanics* **659**, 267–288.
- Ihme, M., Pitsch, H. & Bodony, D. 2009 Radiation of noise in turbulent non-premixed flames. *Proceedings of the Combustion Institute* **32**, 1545–1553.
- Jiang, G.-S. & Shu, C.-W. 1996 Efficient implementation of weighted ENO schemes. *Journal of Computational Physics* **126**, 202–228.
- Kee, R. J., Graham, D.-L., Warnatz, J., Coltrin, M. E. & Miller, J. A. 1986 A fortran computer code package for the evaluation of gas-phase, multicomponent transport properties. SANDIA Report No. SAND86-8246. Sandia National Laboratories, Albuquerque NM, Livermore CA.
- Kee, R. J., Rupley, F. M. & Miller, J. A. 1989 Chemkin-II: A FORTRAN chemical kinetics package for the analysis of gas-phase chemical kinetics. SANDIA Report No. SAND89-8009B. Sandia National Laboratories, Albuquerque NM, Livermore CA.
- Kempf, A. M., Wysocki, S. & Pettit, M. 2012 An efficient, parallel low-storage implementation of Kleins turbulence generator for LES and DNS. *Computers and Fluids* **60**, 58–60.
- Kitano, T., Kaneko, K., Kurose, R. & Komori, S. 2016 Large-eddy simulations of gas- and liquid-fueled combustion instabilities in back-step flows. *Combustion and Flame* **170**, 63–78.
- Kitano, T., Nishio, J., Kurose, R. & Komori, S. 2014 Evaporation and combustion of multicomponent fuel droplets. *Fuel* **136**, 219–225.
- Klein, M., Sadiki, A. & Janicka, J. 2003 A digital filter based generation of inflow data for spatially developing direct numerical or large eddy simulations. *Journal of Computational Physics* **186**, 652–665.
- Miller, R. S. & Bellan, J. 1999 Direct numerical simulation of a confined three-dimensional gas mixing layer with one evaporating hydrocarbon-droplet laden stream. *Journal of Fluid Mechanics* **384**, 293–338.
- Miller, R. S., Harstad, K. & Bellan, J. 1998 Evaluation of equilibrium and non-equilibrium evaporation models for many-droplet gas-liquid flow simulations. *International Journal of Multiphase Flow* **24** (6), 1025–1055.
- Moureau, V., Bérat, C. & Pitsch, H. 2007 An efficient semi-implicit compressible solver for large-eddy simulations. *Journal of Computational Physics* **226** (2), 1256–1270.
- Nakamura, M., Akamatsu, F., Kurose, R. & Katsuki, M. 2005 Combustion mechanism of liquid fuel spray in a gaseous flame. *Physics of Fluids* **17** (12), 123301.
- Pillai, A. L., Muto, M. & Kurose, R. 2016 Numerical investigation of effect of Reynolds number on noise from turbulent non-premixed hydrogen jet flames. In *Proceedings of the Asian Congress on Gas Turbines ACGT2016*, p. 23. Mumbai, India: Indian Institute of Technology Bombay.
- Singh, K. K., Frankel, S. H. & Gore, J. P. 2004 Study of spectral noise emissions from standard turbulent nonpremixed flames. *AIAA Journal* **42**, 931–936.
- Strahle, W. C. 1978 Combustion noise. *Progress in Energy and Combustion Science* **4**, 157–176.
- Watanabe, H., Kurose, R., Hwang, S.-M. & Akamatsu, F. 2007 Characteristics of flamelets in spray flames formed in a laminar counterflow. *Combustion and Flame* **148** (4), 234–248.
- Westbrook, C. K. & Dryer, F. L. 1981 Simplified reaction mechanisms for the oxidation of hydrocarbon fuels in flames. *Combustion Science and Technology* **27**, 31–43.